Dalton Transactions

PAPER

View Article Online
View Journal | View Issue

Cite this: *Dalton Trans.*, 2015, **44**, 18492

Hydration and ion pair formation in aqueous Y^{3+}–salt solutions†

Wolfram W. Rudolph*[a] and Gert Irmer[b]

Raman spectra of aqueous yttrium perchlorate, triflate (trifluoromethanesulfonate), chloride and nitrate solutions were measured over a broad concentration range (0.198–3.252 mol L^{-1}). The spectra range from low wavenumbers to 4200 cm^{-1}. A very weak mode at 384 cm^{-1} with a full width at half height at 50 cm^{-1} in the isotropic spectrum suggests that the Y^{3+} – octa-aqua ion is thermodynamically stable in dilute perchlorate solutions (~0.5 mol L^{-1}) while in concentrated perchlorate solutions outer-sphere ion pairs and contact ion pairs are formed. The octa-hydrate, $[Y(OH_2)_8]^{3+}$ was also detected in a 1.10 mol L^{-1} aqueous $Y(CF_3SO_3)_3$ solution. Furthermore, very weak and broad depolarized modes could be detected which are assigned to $[Y(OH_2)_8]^{3+}$(aq) at 100, 166, 234 and 320 cm^{-1} confirming that a hexa-hydrate is not compatible with the hydrated species in solution. In yttrium chloride solutions contact ion pair formation was detected over the measured concentration range from 0.479–3.212 mol L^{-1}. The contact ion pairs in YCl_3(aq) are fairly weak and disappear with dilution. At a concentration <0.2 mol L^{-1} almost all complexes have disappeared. In YCl_3 solutions, with additional HCl, chloro-complexes of the type $[Y(OH_2)_{8-n}Cl_n]^{+3-n}$ (n = 1,2) are formed. The $Y(NO_3)_3$(aq) spectra were compared with a spectrum of a dilute $NaNO_3$ solution and it was concluded that in $Y(NO_3)_3$(aq) over the concentration range from 2.035–0.198 mol L^{-1} nitrato-complexes $[Y(OH_2)_{8-n}(NO_3)l_n]^{+3-n}$ (n = 1,2) are formed. The nitrato-complexes are weak and disappear with dilution <0.1 mol L^{-1}. DFT geometry optimizations and frequency calculations are reported for both the yttrium–water cluster in the gas phase and the cluster within a polarizable continuum model in order to implicitly describe the presence of the bulk solvent. The bond distance and angle for the square antiprismatic cluster geometry of $[Y(OH_2)_8]^{3+}$ with the polarizable dielectric continuum is in good agreement with data from recent structural experimental measurements. The DFT frequency of the Y–O stretching mode of the $[Y(OH_2)_8]^{3+}$ cluster, in a polarizable continuum, is at 372 cm^{-1} in satisfactory agreement with the experimental value.

Received 8th July 2015,
Accepted 20th September 2015

DOI: 10.1039/c5dt02586a

www.rsc.org/dalton

1. Introduction

Yttrium is a silvery-metallic transition metal in group 3 and chemically similar to the lanthanides. Yttrium is almost always found combined with the lanthanides in rare earth minerals but is never found in nature as a free element. The most important use of yttrium is in making phosphors and also in the production of electrolytes, electronic filters, lasers and superconductors.[1–3] Its radioactive isotope, ^{90}Y, has a wide use in radiation therapy to treat cancer.[4] Yttrium has no known biological role though it is found in most, if not all, organisms and tends to concentrate in the liver, kidney, spleen, lungs, and bones of humans.[5] The coordination numbers in crystalline Y^{3+}-compounds vary widely from 3 to 12[6] but eight and nine fold coordination are the most frequent.[7–11]

In aqueous solution, yttrium exists exclusively in the trivalent state, Y^{3+}, and the ion is strongly hydrated judging by its high hydration enthalpy,[3] due to its high charge to radius ratio. The hydration number for Y^{3+} in aqueous solution was determined based on structural techniques such as X-ray diffraction (XRD), anomalous X-ray diffraction (AXD) and large angle X-ray scattering (LAXS).[12–16] The local structure of aqueous Y^{3+} salt solutions was also studied applying extended X-ray absorption fine structure (EXAFS), and X-ray absorption fine structure (XAFS) methods.[17–20] A combined study of neutron scattering and EXAFS measurements applying reversed modeling on YCl_3(aq) must be mentioned.[21] A summary of experimental structural results is presented in Table 1. From the Table, it is clear that Y^{3+} is hydrated by 8 water molecules in the first-shell forming a square-antiprismatic geometry. The Y^{3+}–O bond distance was found at

[a]*Medizinische Fakultät der TU Dresden, Institut für Virologie im MTZ, Fiedlerstr. 42, 01307 Dresden, Germany. E-mail: Wolfram.Rudolph@tu-dresden.de*
[b]*Technische Universität Bergakademie Freiberg, Institut für Theoretische Physik, Leipziger Str. 23, 09596 Freiberg, Germany*
†Electronic supplementary information (ESI) available. See DOI: 10.1039/c5dt02586a

Table 1 Coordination numbers and Y–O bond distances for aqueous Y^{3+}–salt solutions at room temperature (298 K)

Method	Solution composition	La^{3+}/ mol L^{-1}	CN	Y–O bond distance/Å	Remarks	Ref.
XRD	$Y(ClO_4)_3$	1.094	8.0 ± 0.3	2.37 ± 0.005	Second sphere: 4.52 Å	12
	$Y_2(SeO_4)_3$	0.77	8.0 ± 0.3	2.33 ± 0.005	Second sphere: 4.47 Å	
		0.89		2.325 ± 0.005	Second sphere: 4.47 Å	
AXD	YCl_3	0.5	8.1 ± 0.3	2.46 ± 0.02		13
		1.0	8.2 ± 0.5	2.51 ± 0.02		
EXAFS	YCl_3	0.6	7.5 ± 0.3	2.34 ± 0.02	Y K-edge additionally Raman spectra of YCl_3 in H_2O and D_2O are given	17
		1.2	7.6 ± 0.3	2.34 ± 0.02		
		2.3	7.9 ± 0.3	2.34 ± 0.02		
	YBr_3	0.5	7.5 ± 0.3	2.33 ± 0.02		
		1.0	8.5 ± 0.3	2.33 ± 0.02		
		2.1	7.5 ± 0.3	2.34 ± 0.02		
XRD	YCl_3	2.73	7.7 ± 0.3	2.36 ± 0.02		14
	YBr_3	2.67	7.8 ± 0.3	2.36 ± 0.02		
EXAFS	YCl_3	0.1	9.1 ± 0.2	2.36 ± 0.02	Temperature dependent measurements from 25–340 °C	18
	$Y(NO_3)_3$	0.05	9.4 ± 0.2	2.367 ± 0.006		
EXAFS/ LAXS	$Y(ClO_4)_3$ acidified with $HClO_4$	1.71	8.0 ± 0.1	2.368 ± 0.005	Mean value of second hydration sphere consisting of ~16 oxygen atoms at a mean Y–O distance of 4.40(4) Å	19
		1.14				
		0.43				
EXAFS/ XANES	YBr_3	0.005 mol kg^{-1}	8.6 ± 0.1	2.352 ± 0.003	Concentration profile from 0.005–2.00 mol kg^{-1}	20
		2.00 mol kg^{-1}	8.8 ± 0.1	2.353 ± 0.001		
AXD	YCl_3	3.5 mol kg^{-1}	8	2.33	Second sphere at 4.77 YCl_3; conctact ion pairs between Y^{3+} and Cl^-	15
XRD	$Y(NO_3)_3$	2.89	8.0 ± 0.1	2.36 ± 0.01	Additionally Raman spectrum of $Y(NO_3)_3$ in H_2O was given	16
ND/EXAFS	YCl_3	1 mol kg^{-1}	~7.4 ± 0.5 Y–O_w ~0.8 ± 0.2 Y-Cl	2.33	Contact ion pairs between Y^{3+} and Cl^- were established	21

2.366 Å. In addition to the experimental work, a computer simulation significantly contributed to clarifying the details of the structure and dynamics of the waters in the first hydration shell of Y^{3+}.[22] This simulation study confirmed the Y^{3+} octahydrate and its square antiprismatic geometry. Furthermore, the structural results show that X-ray measurements and EXAFS investigations were carried out at high and low solute concentrations using different anions as counter ions. This, however, poses a problem because contact ion pairs may form in concentrated solutions and this fact has been reported in an earlier XRD study on yttrium selenate solutions.[12] A recent notable structural study on an aqueous 1 mol kg^{-1} YCl_3 solution applying a local structure refinement model of disordered material[21] revealed contact ion pairs between Y^{3+} and Cl^-.

Raman spectroscopy which probes the immediate environment of metal ions in solution was frequently used to study hydrated cations by measuring the vibrational modes of a $[M(H_2O)_n]^{x+}$ species.[23–28] A highly polarized band in the 250–550 cm^{-1} region due to the symmetrical metal–oxygen mode of the hydrated cation is the most characteristic peak. This peak is sensitive to possible ion pair formation. Occasionally, all the bands of the metal–oxygen modes may be observed and used to support the assignment of the point group symmetry and coordination number in aqueous solution. Raman scattering measurements on Y^{3+}(aq) should allow, in principle, the characterization of the solution structure in greater detail. However, aqueous Y^{3+} solutions were measured by Raman spectroscopy only on a few occasions.[16,17,29] Due to the limitations of Raman spectroscopic technique at the time, the quality of the spectra in the low frequency range[17,29] was poor. Furthermore, no reduced spectral treatment of the data in the low frequency range was applied. It has been shown on a variety of aqueous metal salt solutions that for meaningful Raman spectroscopic analysis, reduced spectra (spectra in *R*-format) are necessary in the terahertz frequency range[23–28] in order to account for the Bose-Einstein correction and scattering factor.[23,30]

The present study was undertaken to characterize the hydration and speciation in aqueous Y^{3+} solutions and to this end Y^{3+} – salt solutions with common anions (ClO_4^-, $CF_3SO_3^-$, Cl^-, NO_3^-) were studied over a broader concentration range and down to the terahertz frequency range. Triflate and perchlorate are considered non-complex-forming anions and were therefore chosen to measure the Y–O modes in aqueous solution so as to identify and assign bands unique to the first hydration sphere of Y^{3+}(aq). A $Y(ClO_4)_3$ solution in heavy water was also measured in order to characterize the vibrational isotope effect by changing from $[Y(H_2O)_8]^{3+}$ to $[Y(D_2O)_8]^{3+}$. In a variety of di- and trivalent metal ion solutions with chloride and nitrate as counterions, however, it has been shown that these anions readily form complexes[24–28] and the question arises as to whether these complexes also occur with Y^{3+}(aq). Specifically, the following aqueous systems were measured by Raman spectroscopy at 23 °C: $Y(ClO_4)_3$ and

$Y(ClO_4)_3$ plus $HClO_4$, $Y(CF_3SO_3)_3$, YCl_3 and YCl_3 plus additional HCl, and $Y(NO_3)_3$. $Y(ClO_4)_3$ solutions in heavy water were measured not only to determine the isotope effect on the Y–O modes (Y–OH_2/D_2O) but also to measure the influence of the salts on the water and heavy water stretching and deformation bands as a function of the Y^{3+} salt concentration.

Calculations on yttrium–water clusters with six and eight waters in the first sphere were considered applying density functional theory (DFT) in the gas phase. However, gas phase clusters do not reflect the aqua-cluster geometry nor the vibrational modes of metal ions in solution[23–28] and therefore, Y^{3+}– clusters with a polarizable dielectric continuum were simulated in order to take into account the effects of the bulk solvent. Frequency calculations were carried out *via* the calculation of the second derivative of the energy with respect to the nuclear positions of Y^{3+}–water clusters.

2. Experimental details; data analysis and DFT calculations on Y^{3+}–water clusters

A. Preparation of solutions

The yttrium ion concentrations of all solutions were analysed by complexometric titration.[31] The solution densities were determined with a pycnometer at 23 °C and the molar ratios water per salt were calculated (R_w-values). For Raman spectroscopic measurements the solutions were filtered through a fine sintered glass frit (1–1.6 μm pore size). The solutions showed no Tyndall effect and were "optically empty".[32]

Yttrium perchlorate solutions were prepared from Y_2O_3 (Sigma-Aldrich, 99.9%) and $HClO_4$ in a beaker until all oxide dissolved. A $Y(ClO_4)_3$ stock solution was prepared at 2.559 mol L^{-1} (R_w = 16.25). This solution was acidified with a slight amount of $HClO_4$ and a pH value at ~3.5 for the concentrated solutions was measured. From this stock solution, the following dilution series was prepared: 2.378 mol L^{-1} (R_w = 21.46), 1.785 mol L^{-1} (R_w = 25.67), 1.280 mol L^{-1} (R_w = 37.81), 0.853 mol L^{-1} (R_w = 59.45), 0.640 mol L^{-1} (R_w = 81.10) and 0.256 mol L^{-1} (R_w = 210.9). The solutions were analysed for dissolved chloride with a 5% $AgNO_3$ solution. The absence of a white AgCl precipitate was proof that the stock solution was free of Cl^-.

Two $Y(ClO_4)_3$ solutions in heavy water were prepared from a deuterated $Y(ClO_4)_3$ stock solution and with 99.9 atom % D (Sigma-Aldrich) at 2.30 mol L^{-1} and 1.73 mol L^{-1}.

A 1.10 mol L^{-1} $Y(CF_3SO_3)_3$ solution was prepared from anhydrous $Y(CF_3SO_3)_3$ (Sigma-Aldrich, 99.9%) and triply distilled water.

Seven YCl_3 solutions were prepared from $YCl_3{\cdot}6H_2O$ (Sigma, 99.9%) and triply distilled water. The solution concentrations were found at 3.212 mol L^{-1} (R_w = 15.40), 2.378 mol L^{-1} (R_w = 21.46), 2.141 mol L^{-1} (R_w = 24.00), 1.175 (R_w = 45.30), 1.010 mol L^{-1} (R_w = 53.53), 0.803 mol L^{-1} (R_w = 67.19) and 0.479 mol L^{-1} (R_w = 113.82). Furthermore, a solution series with an excess of HCl was prepared (YCl_3 plus HCl): (A) 2.13 mol L^{-1} YCl_3 + 4.03 mol L^{-1} HCl and (B) 2.17 mol L^{-1} YCl_3 + 1.31 mol L^{-1} HCl. Two HCl solutions were also prepared at 3.97 mol L^{-1} and at 1.325 mol L^{-1}.

Three $Y(NO_3)_3$ solutions were prepared from $Y(NO_3)_3{\cdot}6H_2O$ and triply distilled water: 2.035 mol L^{-1} (R_W = 23.04), 1.036 mol L^{-1} (R_W = 49.20) and 0.198 mol L^{-1} (R_W = 275.88).

B. Spectroscopic measurements

Raman spectra were measured in the macro chamber of the T 64000 Raman spectrometer from Jobin Yvon in a 90° scattering geometry at 23 °C. These measurements have been described elsewhere.[30,33] A quartz cuvette from Hellma Analytics (Müllheim, Germany) with 10 mm path length and a volume 1000 μL was used. Briefly, the spectra were excited with the 514.532 nm line of an Ar^+ laser at a power level of 1100 mW at the sample. After passing the spectrometer in subtractive mode, with gratings of 1800 grooves per mm, the scattered light was detected with a cooled CCD detector. I_{VV} and I_{VH} spectra were obtained with fixed polarization of the laser beam by rotating the polarizator at 90° between the sample and the entrance slit to give the scattering geometries:

$$I_{VV} = I(Y[ZZ]X) = 45\alpha'^2 + 4\gamma'^2 \quad (1)$$

and

$$I_{VH} = I(Y[ZY]X) = 3\gamma'^2. \quad (2)$$

The isotropic spectrum, I_{iso} is then constructed:

$$I_{iso} = I_{VV} - 4/3 \cdot I_{VH}. \quad (3)$$

The polarization degree of the Raman bands, ρ ($\rho = I_{VH}/I_{VV}$) was determined using a polarizer and if necessary adjusted before each measuring cycle using CCl_4. A detailed account on this procedure may be found in ref. 30 and 33.

In order to obtain spectra defined as $R(\bar{\nu})$ which are independent of the excitation wavenumber ν_L, the measured Stokes intensity should be corrected for the scattering factor $(\nu_L - (\bar{\nu}))^3$. In the case of counting methods used, the measured count rates were corrected with the factor $(\nu_L - (\bar{\nu}))^3$. The spectra were further corrected for the Bose-Einstein temperature factor, $B = [1 - \exp(-h\bar{\nu}c/kT)]$ and the frequency factor, $\bar{\nu}$, to give the so called reduced spectrum, $R(\bar{\nu})$. It is also possible to calculate the isotropic spectrum in *R*-format from the corrected R_{VV} and R_{VH} spectra according to eqn (4):

$$R(\bar{\nu})_{iso} = R(\bar{\nu})_{VV} - 4/3R(\bar{\nu})_{VH.} \quad (4)$$

In the low wavenumber region, the $I(\bar{\nu})$ and $R_Q(\bar{\nu})$ spectra are significantly different and only the spectra in *R*-format are presented. It should be noted that one of the advantages of using isotropic R-spectra is that the baseline is almost flat in the 50–700 cm^{-1} wavenumber region allowing relatively unperturbed observation of the presence of any weak modes.[23,30,33]

C. DFT calculations

The calculations were carried out using the Gaussian03 package[34] employing the unrestricted B3LYP functional.[35] The LANL2DZ (Los Alamos National Laboratory 2 Double Zeta) basis set was used which adequately reproduces the geometrical parameters, in particular the experimentally observed Y–O distance. LANL2DZ uses a relativistic effective core potential (ECP) for the inner electrons of Y^{3+}, and its valence electrons. All electrons for the other atoms are described by D95 V (Dunning/ Huzinaga valence double-zeta) functions. The 6-31G (double-zeta Pople type) basis set and application of diffuse and polarization functions for the atoms O and H resulted in small changes. Placing the cluster in a solvent continuum employing the Polarized Continuum Model (PCM) which takes into account the solvation effect of bulk water gave significantly better results compared with the experimental frequencies. The PCM used was the version described in ref. 36 where the solvent is modelled as an isotropic and homogeneous continuum, characterized by its dielectric properties. The cavity is defined as a set of interlocking spheres attached to the solute atoms. The electrostatic solute–solution interaction is calculated introducing an apparent charge distribution spread on the cavity surface.

Geometries of gas phase clusters with 8 water molecules surrounding the Y^{3+} ion, were optimized applying different basis sets and several cluster geometries for $[Y(H_2O)_8]^{3+}$ with different symmetries namely D_4, C_2 and S_8 were considered. A $[Y(H_2O)_8]^{3+}$ cluster with symmetry S_8 including a polarizable dielectric continuum (PC) was simulated in order to take into account the solvent effect. The cluster with S_8 symmetry was the only cluster which led to an energy minimum without imaginary frequencies. The frequencies of the $[Y(H_2O)_8]^{3+}$ cluster including a polarizable dielectric continuum were calculated (B3LYP/LANL2DZ). The DFT simulations on $[Y(H_2O)_6]^{3+}$ gave a stable geometry with symmetry T_h. The $[Y(H_2O)_6]^{3+}$ cluster imbedded in a PC was optimized and frequencies were calculated. The geometric data and the frequency of the breathing mode of the $[Y(H_2O)_8]^{3+}$ cluster in comparison with the $[Y(H_2O)_6]^{3+}$ will be discussed below.

3. Results and discussion

3.1. The $[Y(OH_2)_8]^{3+}$(aq) ion

Y^{3+} is strongly hydrated in aqueous solution as indicated by its large standard molar enthalpy of hydration (ΔH^o_{hyd}) at ~ -3640 kJ mol^{-1} but it should be stressed that ΔH^o_{hyd} – values reported in the literature scatter from -3583 to -3733 kJ mol^{-1}.[37–42] Our DFT value for ΔH^o_{hyd} is -3951 kJ mol^{-1} which is smaller than the thermodynamic value (calculation procedure in Appendix A). The Y^{3+} ion, hydrated by eight water molecules in the first hydration shell with a Y–O bond distance at 2.366 Å, and a second hydration shell, much more diffuse, at 4.40 Å consisting of ~16 water molecules was observed.[19] The optimized $[Y(H_2O)_8]^{3+}$ geometry in the gas phase and also with a polarizable continuum gave a square antiprismatic YO_8 coordination polyhedron with symmetry S_8 (Fig. 1). The cluster, $[Y(H_2O)_8]^{3+}$, was also optimized applying higher basis sets which led to geometries with symmetry D_4 and C_2 (Table S1†). However, only the $[Y(H_2O)_8]^{3+}$ cluster with S_8 symmetry imbedded in a PC could be successfully simulated. The calculated Y–O bond distance of the $[Y(H_2O)_8]^{3+}$ cluster with a solvation sphere, taking into account the influence of the bulk water, is in good agreement with the experimental value (Table 1). The $[Y(H_2O)_8]^{3+}$ cluster in the gas phase, however, shows a larger value compared to the experimental Y–O bond distance (lack of bulk water). These DFT results are given in Table 2 together with the experimental data and a Car–Parrinello molecular dynamics (CPMD) simulation result.[22]

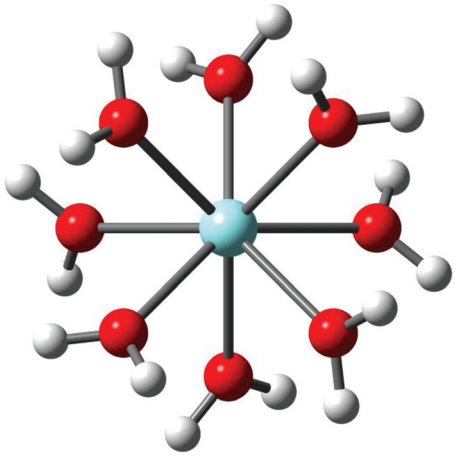

Fig. 1 Structure of the octa-aqua Y^{3+}-ion (S_8 – symmetry).

A Y^{3+}-hexa-hydrate was also successfully optimized but a noticeably smaller Y–O bond distance (Table S2†) was found compared to the measured one at 2.366 Å (ref. 19) which shows that the hexa-hydrate may be ruled out as a valid species in aqueous solution.‡ The results for the $[Y(H_2O)_6]^{3+}$ in the gas phase and modelled with a solvation sphere are also given in Table S2.† (In contrast to solution state, in crystalline compounds CNs vary from 3–12.[3,6])

The *vibrational analysis* of the $[Y(OH_2)_8]^{3+}$ (S_8 symmetry) with its 69 normal modes (n.m.'s) leads to the following irreducible representation: $\Gamma_v(S_8)$ = 8a(Ra) + 9b(i.r.) + 18e$_1$(Ra, i.r.) + 18e$_2$ (n.a.) + 16e$_3$ (n.a.). The modes with character a and e$_1$ are Raman active and those with character b and e$_1$ are infrared active. The vibrations can be divided into 48 internal and external vibrations of the eight coordinated water molecules plus 21 n. m.'s of the YO_8 skeleton.

The vibrations of the water modes are decoupled from those of the YO_8 skeleton and the water molecules of the first shell are considered point masses. The YO_8 skeleton (D_{4d} symmetry) with its 9 atoms leads to 21 n.m.'s. The irreducible representation of these skeleton modes is as follows: $\Gamma_v(D_{4d})$ = 2a$_1$ (Ra) + b$_1$(i.a.) + 2b$_2$(i.r.) + 3e$_1$(i.r.) + 3e$_2$(Ra) + 2e$_3$(Ra). Although

‡ In early literature[29] a Y^{3+}-hexahydrate was assumed in the solution state.

Table 2 Geometrical parameters such as bond distances and bond angles of $[Y(H_2O)_8]^{3+}$ imbedded in a polarizable dielectric continuum. Comparison of the DFT results (B3LYP/LANL2DZ) with published MD simulation and experimental results

Bond distances (Å) and angels (°)	DFT data/ gas phase cluster	DFT data/ cluster + PC model	Ref. 22 [a]	Ref. 12 [b]	Ref. 19 [c]	Ref. 18 [d]
Y–O	2.399	2.354	2.38	2.37	2.368	2.618
O–H	0.981	0.989	0.96			
H–O–H	109.6	110.9	106			

[a] CPMD; O–H bond distance and H–O–H angle from Fig. 5.[22] [b] XRD: results for $Y(ClO_4)_3$(aq). [c] EXAFS: results for $Y(ClO_4)_3$(aq). [d] EXAFS: results on diluted YBr_3(aq).

the YO_8 skeleton possesses no symmetry centre, the mutual exclusion rule is nevertheless effective. The 7 modes with the character a_1, e_2 and e_3 are Raman active while the six modes with the character b_1, b_2 and e_1 are infrared allowed. The symmetric Y–O stretch, the breathing mode, is only Raman active and appears strongly polarized in the Raman spectrum as the strongest band of the skeleton. Two additional depolarized Raman active stretching modes are expected (character e_2 and e_3) as well as four other Raman deformation modes (character a_1, e_2 and e_3). In I.R., two stretching modes (character b_2 and e_1) are expected and the remaining are deformations. In reality, however, the skeleton modes may not always be easily detected because they appear quite broad, weak and even obscured.

Considering the coordinated water molecules of the $[Y(OH_2)_8]^{3+}$ cluster, the internal and external n.m.'s of the water molecules may be divided into 24 internal and 24 external vibrations. These vibrations are derived from the rotational- and translational degrees of freedom of the isolated water molecule. The n.m.'s of these waters, the external modes, are librations such as wag, twist, and rock.[43] Generally, the water molecules in the metal-aqua complexes possess weak, very broad modes below 1200 cm^{-1}. In addition to these librations, internal water modes are observed: the deformation mode, $\nu_2(H_2O)$ and two stretching OH modes, ν_1 and ν_3. The deformation mode in liquid water is found at 1640 cm^{-1} and the stretching modes at ~3400 cm^{-1} appear as a very broad structured band of H-bonded water molecules. The water modes are modified when coordinated to metal ions such as Y^{3+} but are difficult to separate from the contributions of the librational and internal water modes of the bulk phase. In neat liquid water, the H-bonded water molecules show broad and weak librational modes and internal water modes, the deformation band, δ H–O–H, and the stretching O–H bands.[43] Spectra of liquid water and heavy water, bands and band assignments are given elsewhere.[44–46]

The hydration sphere of Y^{3+}(aq) is somewhat labile and a water-exchange rate constant k_{ex} at 25 °C was given at 2×10^7 s^{-1} (from H_2O–SO_4^{2-} interchange rates) with a water residence time τ = 50 ns. The hydration sphere of Y^{3+}(aq), however, is less labile compared to $[La(OH_2)_9]^{3+}$(aq).[47,48] § The mechanistic path for the water exchange for $[Ho(OH_2)_8]^{3+}$ follows an associative water exchange process.[51–53] It is safe to assume a similar water exchange mechanism for Y^{3+}(aq) because of its similar ionic radius compared to Ho^{3+}(aq).[54]

Chemically, yttrium resembles the heavy rare earth elements more closely than scandium,[3,6] its neighbor in the periodic table, and especially holmium in its chemical behavior.[3] Y^{3+}(aq) is less basic in aqueous solution ($\log K_{h,1} = -7.8$) compared to La^{3+}(aq) ($\log K_{h,1} = -8.81$).[55] A first principle MD simulation on the stepwise hydrolysis reaction of Y^{3+} in aqueous solution has been presented recently.[56]

3.2. $Y(ClO_4)_3$ and $Y(CF_3SO_3)_3$ solutions in water and heavy water

$Y(ClO_4)_3$ solution spectra. An overview Raman spectrum of a 1.28 mol L^{-1} $Y(ClO_4)_3$ solution (R_w = 37.7) is presented in Fig. 2 and additionally the Raman spectrum of a 0.256 mol L^{-1} solution (R_w = 211) in the terahertz frequency range in Fig. S1.† The perchlorate ion has been chosen as a counterion because it is known as a non-complex ion which is only weakly hydrated. A high frequency band at 3538 cm^{-1} (fwhh = 90 cm^{-1}) is observed in $Y(ClO_4)_3$ solutions which is attributed to an O–H band weakly hydrated perchlorate ion¶ (Fig. 2, lower panel). A concentration profile of $Y(ClO_4)_3$ solutions in comparison with the OH stretching profile of neat water is given in Fig. S2.† The decoupled O–H oscillator of HDO for a 2.559 mol L^{-1} $Y(ClO_4)_3$ solution appears at 3563 cm^{-1} and Raman profiles of the polarized, depolarized and isotropic scattering are given in Fig. S3.† For a detailed discussion on the influence of ClO_4^- on the stretching band of water in, for instance, $Ca(ClO_4)_2$(aq) see ref. 24. It is noteworthy to mention that the stretching band of O–H···$OClO_3^-$ is slightly cation dependent which is caused by their different charge to radius ratios (polarizing power). In $Y(ClO_4)_3$(aq), the band appears at 3538 cm^{-1}, slightly lower than in $Ca(ClO_4)_2$(aq) where it shows at 3550 cm^{-1}.[24] The ν O–D···$OClO_3^-$ band in solutions of $Y(ClO_4)_3/D_2O$ solution appears at 2583 cm^{-1} with the Raman spectrum given in Fig. S4.†

The ClO_4^- ion (T_d symmetry) has nine vibrational degrees of freedom and its internal vibrations span the representation $\Gamma_{vib}(T_d) = a_1(Ra) + e(Ra) + 2f_2(Ra, i.r.)$. All four n.m.'s are Raman active, but in i.r. only the f_2 modes are active. The Raman and infrared spectra of ClO_4^-(aq) are well characterized[24–26] and therefore shall be only, briefly, discussed. In dilute solution, the symmetric Cl–O stretch, $\nu_1(a_1)$

§ The vibrational duration for the Y–O breathing mode is 0.09 ps. Approximately ~5.6×10^5 vibrations occur before the cluster experiences a water exchange.

¶ In addition to the stretching mode ν(O–H···ClO_4^-) at 3538 cm^{-1} a very weak, broad mode appears in the terahertz region at ~170 cm^{-1} in $Y(ClO_4)_3$ solutions (R_{iso}) as very broad and very weak. This mode has an equivalent in pure water at ~175 cm^{-1} where it is moderately intense and slightly polarized (restricted translational mode of the H-bonded water molecules (O···O–H)). In concentrated $Y(ClO_4)_3$ solutions other H-bonds are important, namely OH···ClO_4^- and the intensity of the band due to HOH···ClO_4^- is extremely weak in the isotropic Raman scattering.[24,49,50]

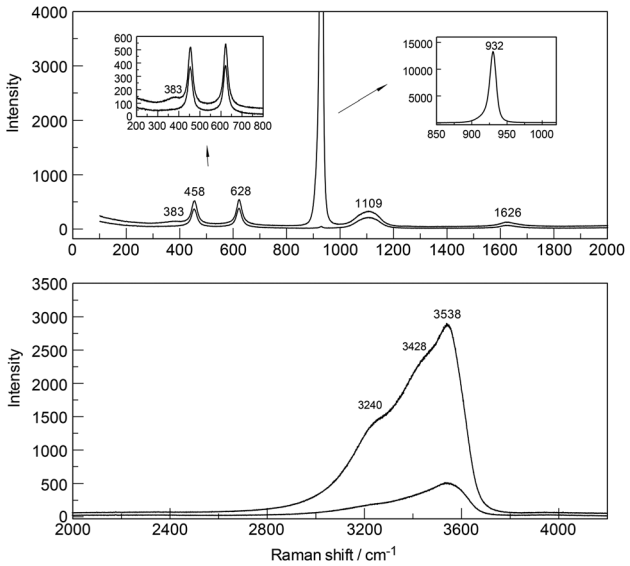

Fig. 2 Overview Raman spectrum (polarized and depolarized) of a 1.28 mol L^{-1} $Y(ClO_4)_3$ solution (R_w = 37.7). Upper panel: bands of ClO_4^-(aq) and the water deformation mode at 1626 cm^{-1}. The inset at the LHS shows spectra in the terahertz frequency rage in greater detail. The inset at the RHS shows the $\nu_1(a_1)$ ClO_4^- band at full detail. Lower panel: OH-stretching band of water and the O–H···O* band of the weakly H-bonded water, $ClO_4^-\cdots H_2O$ at 3538 cm^{-1}. The peak positions of the O–H water bands are given at 3240 and 3428 cm^{-1}.

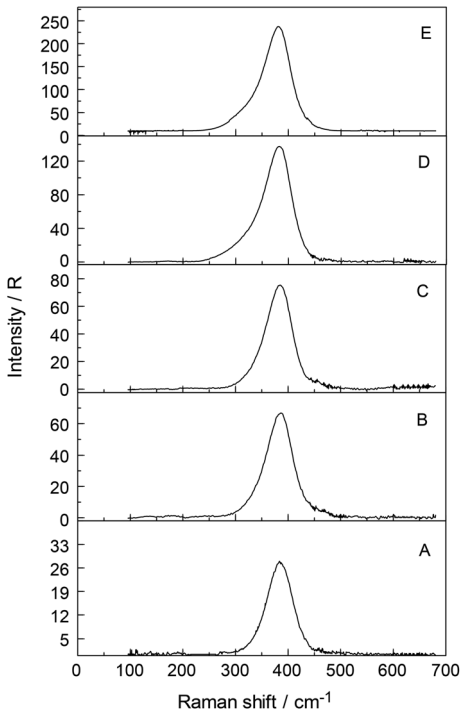

Fig. 3 Concentration plot of isotropic Raman spectra (R-format) of five $Y(ClO_4)_3$ solutions. From bottom to top: (A) 0.256 mol L^{-1} (R_w = 211.0), (B) 0.640 mol L^{-1} (R_w = 81.4), (C) 0.853 mol L^{-1} (R_w = 59.3), (D) 1.280 mol L^{-1} (R_w = 37.7) and (E) 2.559 mol L^{-1} (R_w = 15.7). Note, that the peak position of the YO_8 breathing mode at 384 cm^{-1} for a 0.256 mol L^{-1} solution shifts only slightly to lower wavenumbers at 382 cm^{-1} for a 2.559 mol L^{-1} $Y(ClO_4)_3$ solution. At the same time, the band broadens and a shoulder at 336 cm^{-1} appears for the two most concentrated solutions.

ClO_4^- appears at 931.5 cm^{-1}, is totally polarized (ρ = 0.005) and has a band width equal to 7.1 cm^{-1}. The antisymmetric stretch, $\nu_3(f_2)$ ClO_4^- centred at 1105 cm^{-1} and the deformation modes $\nu_4(f_2)$ ClO_4^- at 629 cm^{-1} and $\nu_2(e)$ ClO_4^- at 458 cm^{-1} are depolarized. In a $Y(ClO_4)_3$ solution at 0.256 mol L^{-1} , the $\nu_1(a_1)$ ClO_4^- band, the strongest Raman band, appears at 931.8 cm^{-1} (fwhh at 7.4 cm^{-1}), shifts to 934.5 cm^{-1} and broadens considerably (fwhh = 13.1 cm^{-1}) in a solution of 2.559 mol L^{-1}. At the same time, the antisymmetric stretch, $\nu_3(f_2)$ ClO_4^- shifts to slightly higher wavenumbers and broadens. The concentration behavior of the ClO_4^- modes in a similar system, $La(ClO_4)_3$(aq), is given in ref. 25.

The Raman spectra of $Y(ClO_4)_3$(aq) reveal, in addition to the perchlorate-bands, weak bands in the terahertz frequency region in the R_{VV} orientation which will be discussed further below (Fig. 2, upper panel). In the isotropic scattering profile, a band appears at 384 cm^{-1} but does not exist in $NaClO_4$(aq) or $HClO_4$(aq). The band must therefore stem from vibrations connected to the YO_8 skeleton. This strongly polarized band is assigned to the symmetric stretching mode, the breathing mode of the $[Y(OH_2)_8]^{3+}$ cluster. In a fairly dilute $Y(ClO_4)_3$ solution at 0.256 mol L^{-1} the band appears symmetrical with a fwhh = 50 cm^{-1} (Fig. S1†). With increasing $Y(ClO_4)_3$ concentration, it widens and shifts to slightly lower wavenumbers. In a concentrated solution at 2.559 mol L^{-1}, the breathing mode, ν_1YO_8 of the $[Y(OH_2)_8]^{3+}$ cluster appears at 382 cm^{-1}. The concentration profiles of the isotropic breathing mode, YO_8 is shown in Fig. 3. The integrated band intensity of this ν_1YO_8 mode, depending on the $Y(ClO_4)_3$ solute concentration, plots as a straight line and the linear function: $A_{384} = 1331.2 \cdot C_0$ (coefficient of determination, R^2 = 0.997) with A_{384} the integrated band intensity of ν_1YO_8 and C_0 the stoichiometric $Y(ClO_4)_3$ concentration. Replacing water with heavy water leads to an isotope shift to lower wavenumbers by a factor of ~0.948 in $Y(ClO_4)_3(D_2O)$. The effect of deuteration on the YO_8 breathing mode was measured in $Y(ClO_4)_3$–D_2O solutions and a band at 365 cm^{-1} observed. The theoretical shift of ν_1 on deuteration (H_2O/D_2O considered as point masses) is given according to:

$$\nu'_1 = \nu_1[m(H_2O)/m(D_2O)]^{1/2} = (384\ cm^{-1}) \cdot 1.054 = 364.2\ cm^{-1}. \quad (5)$$

Relative intensity measurements confirm that the scattering intensity of the ν_1Y–O mode is very weak with the scattering coefficient, S_h = 0.0380. The S_h values, defined as the R-corrected relative scattering efficiency of the M–O bands, were published for a variety of stretching modes of hexa-aqua metal ions in solution.[24,25,27,28] The ν_1 breathing mode for

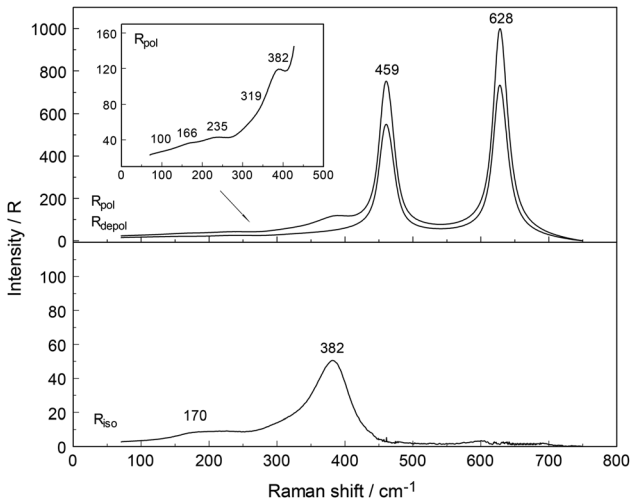

Fig. 4 Raman scattering profiles (R_{VV} and R_{VH}) of a 2.559 mol L^{-1} $Y(ClO_4)_3$ solution (R_w = 15.7). Upper panel: polarized and depolarized scattering profiles dominated by the ClO_4^-(aq) deformation bands at 459 cm^{-1} and 628 cm^{-1}. The inset shows the very weak, depolarized scattering contributions at 100, 166, 235, 319 cm^{-1} and the strongly polarized band 382 cm^{-1} in the polarized scattering ($R_{VV} = 45\alpha'^2 + 4\gamma'^2$). Lower panel: isotropic scattering profile (R_{iso}) showing the breathing mode, ν_1 YO_8 and the weak and broad restricted translational band at ~170 cm^{-1}.

Table 3 The Raman data of the YO_8 skeleton modes of $[Y(H_2O)_8]^{3+}$(aq) and $[Y(D_2O)_8]^{3+}(D_2O)$ taken from an aqueous 2.559 mol L^{-1} $Y(ClO_4)_3$ solution and a 2.30 mol L^{-1} $Y(ClO_4)_3$ solution in heavy water

$[Y(H_2O)_8]^{3+}$			$[Y(D_2O)_8]^{3+}$		
Peak position/ cm^{-1}	Band area	fwhh/ cm^{-1}	Peak position/ cm^{-1}	Band area	fwhh/ cm^{-1}
100.5 (dp)	78	50	90 (dp)	33.5	76
166 (dp)	696	87.5	143 (dp)	138	69.8
233.5 (dp)	570	63	221 (dp)	189	63
319.5 (dp)	331	67	302.5 (dp)	131	53
382 (pp)	3410	58	365 (pp)	2050	53

dp = depolarized mode; pp strongly polarized.

$[La(H_2O)_9]^{3+}$ at 343 cm^{-1} (ref. 26) also possesses a small relative intensity of 0.025. Both ions, Y^{3+} and La^{3+}, have a low polarizability and are classified as hard cations according to the HSAB concept of Pearson.[57]

In addition to the breathing mode of the $[Y(OH_2)_8]^{3+}$ cluster, four other modes appear at 100.5, 166, 233.5 and 319.5 cm^{-1} in the anisotropic scattering (Fig. 4). These weak, broad modes stem from the YO_8 skeleton fundamentals of the $[Y(OH_2)_8]^{3+}$ and break the symmetry of the YO_8 skeleton and therefore appear only in the anisotropic scattering but not in the isotropic profile. These depolarized modes were also observed slightly down-shifted in $Y(ClO_4)_3(D_2O)$ which is caused by the isotope effect going from $[Y(OH_2)_8]^{3+}$ to $[Y(OD_2)_8]^{3+}$. In $[Y(OD_2)_8]^{3+}(D_2O)$ these bands appear at 90, 143, 221, and 302.5 cm^{-1}. The isotope effect on the coordinated heavy water modes was calculated according to eqn (5), however, ν_1 was substituted with ν_i (where index i denotes the frequency of the depolarized YO_8 modes). Table 3 shows the summarized band parameters of the five observed skeleton modes of YO_8 in water and heavy water. From these Raman spectroscopic results, it follows directly that the Y^{3+} hydration shell cannot constitute a hexa-hydrate with T_h symmetry which has been, for instance, characterized for $[Al(OH_2)_6]^{3+}$(aq).[43,58] Group theoretical considerations expect only three skeleton modes in Raman; one of which should be totally polarized (breathing mode for the AlO_6 skeleton) and the remaining two depolarized. All of these bands were detected in the Raman spectrum of an $Al(ClO_4)_3$ solution with the symmetric stretching mode of $[Al(OH_2)_6]^{3+}$ at 525 cm^{-1} strongly polarized and the other two at 438 cm^{-1} and 332 cm^{-1} depolarized.[43,58]

Although the perchlorate ion was chosen as the counter ion because it is known as a non-complexing anion, penetration into the first hydration sphere of the Y^{3+} seems plausible in the most concentrated $Y(ClO_4)_3$(aq). In the $Y(ClO_4)_3$(aq) at 2.559 mol L^{-1} the mole ratio solute to water is 16.3. This water content is enough to completely hydrate the Y^{3+} ion with 8.3 water molecules remaining. It is clear that in these concentrated solutions solvent – separated ion pair formation is simply forced on Y^{3+} because of the lack of water. At such a concentration state the outer-sphere ion pairs, $[Y(OH_2)_8]^{3+}\cdot ClO_4^-$, may exist in equilibrium with contact ions pairs ($Y^{3+}\cdot ClO_4^-$). These ion pairs may explain the slight concentration dependence of the peak position, the shoulder at 336 cm^{-1} mentioned previously and the broadening of the ν_1YO_8 band. In a 0.256 mol L^{-1} $Y(ClO_4)_3$ solution, however, the ν_1YO_8 band occurs as a symmetrical band at 384 cm^{-1} and a fwhh at ~50 cm^{-1}. Furthermore, to rule out a hydrolysis effect, ternary solutions $Y(ClO_4)_3/HClO_4/H_2O$ were studied. $Y(ClO_4)_3$ solution at 2.160 mol L^{-1} plus 1.518 mol L^{-1} $HClO_4$ and a more dilute one at 1.080 mol L^{-1} $Y(ClO_4)_3$ plus 0.759 mol L^{-1} $HClO_4$ were measured in the terahertz frequency range in order to check the influence of the hydrolysis of Y^{3+}(aq). Isotropic bands at 382.5 and 381.5 cm^{-1} appeared with a 15% larger band width than those in $Y(ClO_4)_3$(aq) without additional $HClO_4$. This result shows that the hydrolysis of Y^{3+} cannot be the reason for the variation of the band parameters such as peak position and fwhh of the isotropic Y–O mode and reinforces the assumption of contact-ion-pair formation in the most concentrated solutions.

The DFT frequency of the ν_1YO_8 for $[Y(H_2O)_8]^{3+}$ imbedded in a polarizable dielectric continuum simulating the bulk water phase was calculated at 372 cm^{-1} in satisfactory agreement with the measured value (Table 3) and in contrast to the breathing mode for the cluster in the gas phase at 336.5 cm^{-1}. Imbedding the $[Y(H_2O)_8]^{3+}$ species in a PC to simulate the bulk water is necessary to achieve acceptable agreement with the experimental frequencies. The DFT frequency of the ν_1YO_8 mode for $[Y(D_2O)_8]^{3+}$ imbedded in a PC was calculated at

351 cm^{-1} and in satisfactory agreement with the measured value at 365 cm^{-1} (Table 3). DFT frequencies for the whole $[Y(H_2O)_8]^{3+}$ cluster which includes YO_8 skeletal, librational and internal water modes are given in Table S3 ESI.† The Y–O bond distance of the $[Y(H_2O)_8]^{3+}$ is 2.354 Å in good agreement with the experimental structural data (Table 1).

Similar cluster calculations on Y^{3+} with 6 water molecules surrounded by a polarizable dielectric continuum lead to a stable cluster geometry $[Y(H_2O)_6]^{3+}$ which possesses T_h symmetry. The Y^{3+}-hexa-hydrate has a much shorter Y–O bond distance at 2.28 Å. The DFT frequency for the breathing mode, ν_1YO_6 at 408 cm^{-1} is 7% higher than the experimental one. These results on the $[Y(H_2O)_6]^{3+}$ cluster show that the hexa-hydrate can be ruled out as a valid cluster geometry for Y^{3+} in solution. The ν_1YO_6 frequency, geometrical parameters and the electronic energy of the cluster $[Y(H_2O)_6]^{3+}$ with a solvation sphere, modelled with a PC and for comparison with a gas phase cluster (no bulk-sphere taken into account) are given in Table S3.† To reiterate, the DFT results for $[Y(H_2O)_8]^{3+}$ are in better agreement with the experimental data than for $[Y(H_2O)_6]^{3+}$.

The Raman spectroscopic analysis clearly shows that in dilute $Y(ClO_4)_3$(aq) a mode appears at 384 cm^{-1} (fwhh = 50 cm^{-1}) which represents the breathing mode of the YO_8 skeleton. However, four additional weak and broad bands, depolarized in character, could be characterized in concentrated $Y(ClO_4)_3$(aq). The five bands observed in $Y(ClO_4)_3$(aq) show that the Y^{3+} cannot form a hexa-hydrate in aqueous solution. In concentrated $Y(ClO_4)_3$(aq) > 1.5 mol L^{-1}, outer-sphere ion pair formation is observed indicated by the slight shift of the ν_1YO_8 mode, an asymmetry at 336 cm^{-1}. DFT simulations support the existence of the $[Y(H_2O)_8]^{3+}$ cluster and the calculated breathing mode of the cluster is in satisfactory agreement with the measured one.

3.2.2 Y^{3+}-trifluoromethanesulfonate in aqueous solution. In $Y(CF_3SO_3)_3$(aq) the Y–O band is slightly overlapped with a polarized triflate band at 319 cm^{-1} and appears at ~384 cm^{-1}. The Raman spectrum is shown in Fig. S5.† A band separation resulted in two bands with the first band component at 319 cm^{-1} and the second band at 384 cm^{-1} (fwhh = 48 cm^{-1}). The first band, a polarized band, stems from $CF_3SO_3^-$(aq) but the second band is the YO_8 breathing mode of $[Y(H_2O)_8]^{3+}$. The triflate in aqueous solution acts as a non-complexing anion and is suited therefore for studying metal ion hydration. Band parameters and assignments of $CF_3SO_3^-$(aq) modes are given in Table S4.†

3.3. YCl_3(aq)

An overview Raman spectrum of a 3.212 mol L^{-1} YCl_3 solution (R_w = 15.37) is presented in Fig. 5 and 6 from 100–4200 cm^{-1}. Additionally, concentration plots of four YCl_3(aq) solution spectra from 2.378 to 0.479 mol L^{-1} are presented in the low frequency region of the spectrum (50–1100 cm^{-1}) in Fig. S6† and the O–H stretching region of the solvent, water, in Fig. S7† (2500–4200 cm^{-1}). The broad bands in Fig. 5 in the polarized scattering at 189 cm^{-1}, which is overlapped with a component

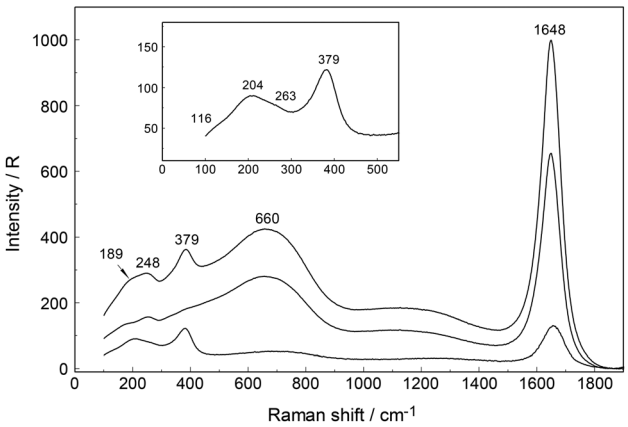

Fig. 5 Raman scattering spectra (*R*-format) of a 3.212 mol L^{-1} YCl_3 solution. The two top curves are the polarized and depolarized scattering profiles and the lower curve represents the isotropic scattering. The Y–O breathing mode to 379 cm^{-1} is slightly downshifted compared to the one in $Y(ClO_4)_3$(aq) at 384 cm^{-1} which is caused by the penetration of Cl^- into the first hydration sphere, forming a species. In the polarized scattering profile, the mode at 248 cm^{-1} is due to an anisotropic $[Y(OH_2)_{8-n}Cl_n]^{+3-n}$ skeleton vibration and the broad overlapped band at 189 cm^{-1} to the restricted translation of water/Cl^-(aq). The extremely broad mode at 660 cm^{-1} is due to the librational water band. The band at 1648 cm^{-1} is due to the deformation mode of the solvent, water. The inset shows the isotropic Raman spectrum in the terahertz region in greater detail. The mode at 204 cm^{-1} is due to the restricted translational band, O–H···O/Cl^- of water/Cl^-(aq) and the broad feature 263 cm^{-1} is assigned to a ν Y^{3+}–Cl^- mode.

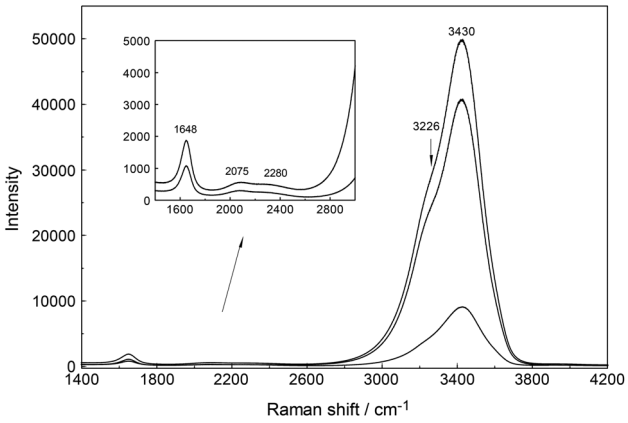

Fig. 6 Raman scattering spectrum (polarized, isotropic (darker line) and depolarized scattering profiles) of a 3.212 mol L^{-1} YCl_3 solution from 1400–4200 cm^{-1}. The inset (only polarized and depolarized scattering) gives the deformation mode at 1648 cm^{-1} and its combination band, which is split into two components at 2075 and 2280 cm^{-1}, of the solvent, water, in greater detail. The O–H stretching band shows two band components at 3226 cm^{-1} and 3430 cm^{-1}.

at 248 cm^{-1} and at 660 cm^{-1} are caused by the solute, water. The broad band at 189 cm^{-1} represents the restricted translation and the band at 660 cm^{-1} librations and a concentration plot in this wavenumber region for four YCl_3 solutions from

2.378 to 0.479 mol L^{-1} is given in Fig. S6.† The deformation band of water appears at 1648 cm^{-1} in the 3.212 mol L^{-1} YCl_3 solution and the O–H profile shows peaks at 3228 cm^{-1} and 3430 cm^{-1} (Fig. 6). Scattering profiles for the same four YCl_3 solutions in the water O–H stretching region at the high frequency range from 2500–4200 cm^{-1} showing the O–H stretching profiles are given Fig. S7.† The influence of the solute YCl_3 on the restricted translation, librations, the H_2O deformation mode and O–H stretching band (Fig. S6 and S7†) with increasing YCl_3 concentration is discussed for a similar system, $CaCl_2$(aq) in greater detail.[24] The similarity of both spectral profiles of $CaCl_2$(aq) and YCl_3(aq) in the O–H stretching region reinforces two facts: one that the O–H stretching profile is mostly influenced by anions, in our case Cl^- and second that Cl^- forms H-bonds of the type O–H···Cl^- almost as strong as the ones between water molecules (O–H···O) in neat water.[24] This stands in contrast to the influence of ClO_4^- on the O–H stretching band of water which forms very weak H-bonds with the solvent as mentioned in section 3.1.

Focusing further on the terahertz frequency region, the Y–O stretching mode in this solution appears at 379 cm^{-1} and is down shifted compared to the unassociated cluster which occurs at 384 cm^{-1}. In addition to the very broad isotropic component at 202 cm^{-1}, mentioned above, a broad shoulder appears at ~263 cm^{-1} and this new isotropic component must stem from a Y^{3+}–Cl^- stretching mode. This finding is clear evidence that Cl^- has penetrated into the first hydration shell of Y^{3+} forming a $[Y(OH_2)_{8-n}Cl_n]^{+3-n}$ (n = 1, possibly 2). With dilution, the Y–O stretching mode shifts to higher wavenumbers from 379 cm^{-1} for a 3.212 mol L^{-1} solution (R_w = 15.4) (Fig. 5) to 384 cm^{-1} obtained in a 0.479 mol L^{-1} solution (R_w = 113.82) (see dilution plot of four YCl_3 spectra from 2.378 to 0.479 mol L^{-1} in Fig. S6†). This fact shows that with dilution of the concentrated solution, the chloro–complex formation disappears rapidly and extrapolation of our Raman data shows that in YCl_3(aq) < 0.2 mol L^{-1} the Y^{3+} cation is fully hydrated. Additionally, the intensity of the band of ν_1YO_8 as a function of concentration does not increase linearly, which would be expected if the octa-hydrated Y^{3+} species remained stable, but curves toward smaller intensities at concentrated solutions. This shows that chloro – complexes must have formed in higher concentrated solutions at the expense of the fully hydrated Y^{3+}, $[Y(H_2O)_8]^{3+}$ (Fig. S8†).

To further verify chloro-complex formation in YCl_3(aq), addition of excess HCl was investigated. Isotropic spectra of YCl_3–HCl solutions at a fixed concentration of YCl_3 at 2.03 mol L^{-1} with 0, 1.0 and 4.0 mol L^{-1} HCl added are shown in Fig. 7. The isotropic band for YCl_3(aq) without added HCl is at 383 cm^{-1}, shifts to 380 cm^{-1} with 1.0 mol L^{-1} HCl added and to 376 cm^{-1} with 4.0 mol L^{-1} additional HCl. The decreasing peak position of the ν_1YO_8 band with increasing HCl concentration reflects the rise in the concentration of the Y^{3+}-chloro-complex, $[Y(OH_2)_{8-n}Cl_n]^{+3-n}$ (n = 1, 2). Fig. 8 presents a difference spectrum of YCl_3(aq) at 2.03 mol L^{-1} plus 4.0 mol L^{-1} HCl(aq) from which the isotropic scattering profile of a 4 mol L^{-1} HCl(aq) was subtracted and reveals broad bands at 326 cm^{-1}, at 228 cm^{-1} and a small scattering contribution at 102 cm^{-1}. Clearly chloro-complexes are formed in these solutions. The formation of the chloro-complex increases with an

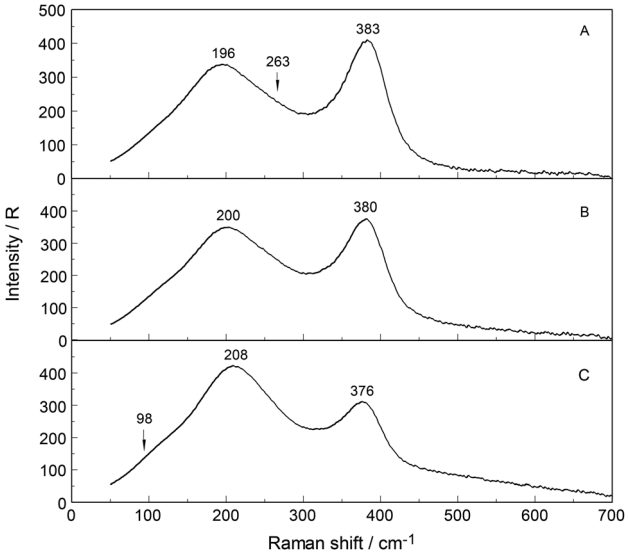

Fig. 7 Isotropic Raman spectra of a 2.13 mol L^{-1} YCl_3 solution and two additional solutions where HCl is added: (A) 2.03 mol L^{-1} YCl_3 without HCl; (B) 2.13 mol L^{-1} YCl_3 + 1.13 mol L^{-1} HCl and (C) 2.13 mol L^{-1} YCl_3 + 3.97 mol L^{-1} HCl. The broad shoulder at 263 cm^{-1} in (A) increases in intensity in solutions B and C and may be assigned to Y^{3+}–Cl^- stretch.

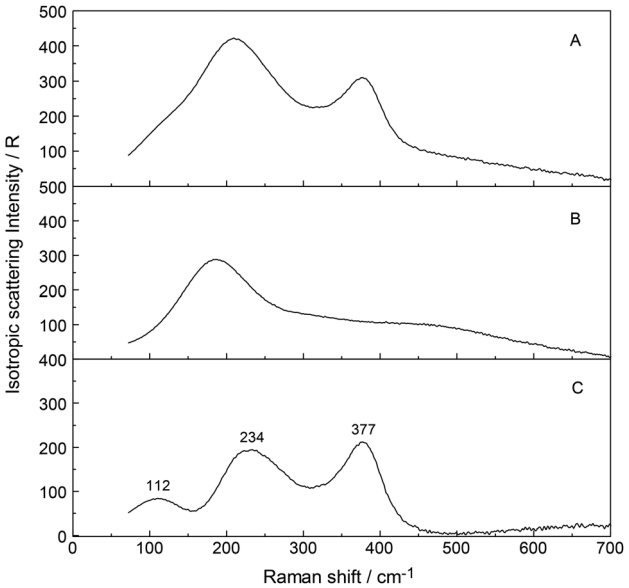

Fig. 8 Difference Raman spectrum (trace in panel C) of the isotropic scattering profile of a 2.13 mol L^{-1} YCl_3(aq) plus 3.97 mol L^{-1} HCl (trace in panel A) from which an isotropic profile of HCl(aq) at 3.98 mol L^{-1} (trace in panel B) was subtracted. Panel C: the band at 377 cm^{-1} stems from the Y–O mode of the complex, $[Y(OH_2)_{8-n}Cl_n]^{+3-n}$ (n = 1,2) and the broad mode at 234 with a shoulder at 263 cm^{-1} and a band at 112 cm^{-1} are due to Y^{3+}–Cl^- vibrations of the chloro-complex species.

increase in Cl^- concentration and the first equilibrium steps according to the eqn (6) may be formulated:

$$[Y(OH_2)_8]^{3+} + Cl^- \leftrightarrow [Y(OH_2)_7Cl]^{2+} + H_2O. \quad (6)$$

Results of anion exchange experiments of metal ions in aqueous HCl(aq) including Y^{3+} showed that yttrium has a negligible adsorption.[59] Therefore, higher Y^{3+}-chloro-complexes (complex anions) with $n > 3$ may be ruled out. The formation of a second complex cation, the di-chloro-complex according to eqn (7) may be possible:

$$[Y(OH_2)_7Cl]^{2+} + Cl^- \leftrightarrow [Y(OH_2)_6Cl_2]^{+} + H_2O. \quad (7)$$

The estimated value of the $\log\beta_1$ for eqn (5) equal to ~0.1 reveals the weak nature of the chloro-complex in YCl_3(aq) at 23 °C. Thermodynamic data on YCl_3(aq) confirm the weak nature of the complex/complexes and equilibrium constants for reaction 6 may be found in ref. 60. The existence of a weak chloro-complex species in $LaCl_3$(aq) using Raman spectroscopy in the terahertz region was presented recently.[26] In the most concentrated YCl_3 solution, the mole ratio solute to water is 1 to 15.4 which means that there are not enough water molecules to form a complete second hydration sphere around all ions forcing outer-shell ion pairing. The chloride ions penetrate the flexible hydration shell of Y^{3+} into the first hydration shell, while in $LaCl_3$(aq) weak chloro-complex formations occur,[26] in $AlCl_3$ solutions, however, even in very concentrated ones, Cl^- does not penetrate into the first hydration shell of Al^{3+}.[43,58] The hydration shell of $[Al(OH_2)_6]^{3+}$ is quite inert. Further experimental support for chloride penetrating into the first hydration shell of Y^{3+} and formation of a chloro-complex stems from a recent combined neutron scattering and X-ray scattering study in which information from EXAFS were incorporated[20] into their applied analytical data treatment. This high quality structural study[21] on a 1.0 mol kg^{-1} YCl_3(aq) showed that Y^{3+} is hydrated by seven water molecules and one chloride ion, forming an inner-sphere ion complex in which the water molecules maintain angular configurations consistent with a square antiprismatic configuration. In an earlier EXAFS study on YCl_3(aq) and YCl_3(aq) plus an excess of LiCl, it was also demonstrated that Cl^- leads to chloro-complex formation in concentrated YCl_3 solutions.[13]

To summarize, the $[Y(OH_2)_{8-n}Cl_n]^{+3-n}$ modes in chloride solutions could be detected and formation of weak chloro-complexes with Y^{3+} were detected. In dilute solutions ($c < 0.2$ mol L^{-1}) the chloro-complex species disappeared upon dilution and $[Y(OH_2)_8]^{3+}$(aq) and Cl^-(aq) are formed. The chloro-complex formation in concentrated solutions may be one reason for the data scatter for Y–O bond distance and coordination numbers presented for Y^{3+}(aq) and this fact was highlighted recently.[21]

3.4. $Y(NO_3)_3$(aq)

When nitrate replaces water in the first coordination sphere of a cation, marked changes occur in the spectrum of the ligated nitrate, so that it is possible to differentiate between the modes of the ligated and the unligated nitrate. Nitrato-complex formation has been observed for a variety of divalent and trivalent metals in solutions.[24–28] The modes of the unligated nitrate, the fully hydrated nitrate, NO_3^-(aq), were measured recently[24–26] and for a 0.409 mol L^{-1} $NaNO_3$ solution (R_W = 134.1) the Raman spectrum is given in ref. 26 together with the vibrational spectroscopic data of the bands and their assignments. Nitrato-complex formation is not only characterized by the ligated NO_3^- but also by the fact that the M–O symmetric stretch of the metal ions (M = metal ion) show two bands, a band of the fully hydrated cation and a band of the partially hydrated metal ion. A ligand mode M–L (L = NO_3^-) should appear at low frequencies as well.

A brief summary for the vibrational data on NO_3^-(aq) shall be presented before discussing the spectroscopic features in $Y(NO_3)_3$(aq). The "free" NO_3^- anion possesses D_{3h} symmetry and four modes should be observed (two doubly degenerate). The n.m.'s span the representation $\Gamma_{vib}(D_{3h}) = a'_1(Ra) + a''_2(i.r.) + 2e'(Ra,i.r.)$. The $\nu_1(a'_1)$ symmetric stretching mode N–O is Raman active but forbidden in infrared, while the e′ modes, ν_3 (N–O antisymmetric stretch) and ν_4 (bending mode) are Raman and infrared active. The out-of plane deformation mode with the character a''_2 is only infrared active. In NO_3^-(aq), the polarized Raman mode at 1047.4 cm^{-1} is the strongest band in Raman scattering and appears quite narrow with a fwhh = 6.55 cm^{-1}. This band is assigned to the symmetric N–O stretch vibration, $\nu_1(a'_1)$. Its depolarization degree at 0.034 is quite low and confirms that it represents a symmetrical normal mode. The mode $\nu_3(e')$, the asymmetric N–O stretching mode which is depolarized and relatively weak appears not as a single band but as two band components at 1347 and 1408 cm^{-1} and appears as a doublet even in very dilute solutions of $NaNO_3$(aq). Asymmetric hydration of the nitrate anion in aqueous solution explains the double band (*cf.* for instance[24,60]). The depolarized mode $\nu_4(e')$ at 716 cm^{-1} is active in Raman and infrared and is much weaker than the symmetric stretching mode $\nu_1(a'_1)$. The infrared active mode, $\nu_2(a''_2)$ occurs at 830 cm^{-1} and its overtone $2 \times \nu_2$ at 1660 cm^{-1} is Raman active (a'_1) and appears polarized.

An overview Raman spectrum (*R*-format) of a 2.035 mol L^{-1} $Y(NO_3)_3$ solution ranging from 40–1800 cm^{-1} is presented in Fig. 9. A concentration series of polarized Raman spectra of three $Y(NO_3)_3$ solutions at 2.035 mol L^{-1} (R_W = 23.04), 1.036 mol L^{-1} (R_W = 49.20) and 0.198 mol L^{-1} (R_W = 257.9) from 100 to 1800 cm^{-1} are presented in Fig. 10. A comparison of Raman spectra of a solution with 2.035 mol L^{-1} $Y(NO_3)_3$ with a solution at 0.198 mol L^{-1} in the low frequency range from 45–900 cm^{-1} is detailed in Fig. S9.† Additionally, in Fig. S10† the same concentrations are compared in the high frequency region from 800–1800 cm^{-1} including the $\nu_3(e')$ antisymmetric stretching region and 2 ν_2 overtone. In these spectra, the nitrate split into bands of free, hydrated nitrate, NO_3^- free and nitrate bound, NO_3^- bound to Y^{3+}. This is a result of the fact that nitrate penetrates into the first hydration sphere forming inner-sphere complexes. The Raman spectra of

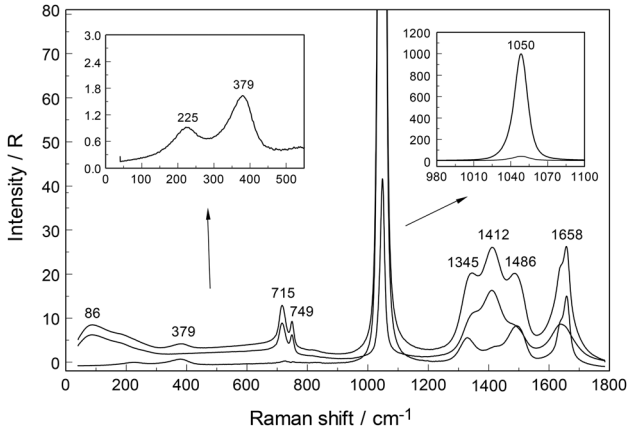

Fig. 9 Raman spectrum of a 2.035 mol L^{-1} (R_W = 23.04) $Y(NO_3)_3$ solution from 45–1800 cm^{-1}. The curves for R_{pol} and R_{depol} scattering are shown on top of R_{iso} (darker, dotted line). The inset at the LHS shows the isotropic scattering at the low wavenumber range while the inset at the RHS depicts the NO_3^-(aq) mode at 1050 cm^{-1} at its full intensity scale.

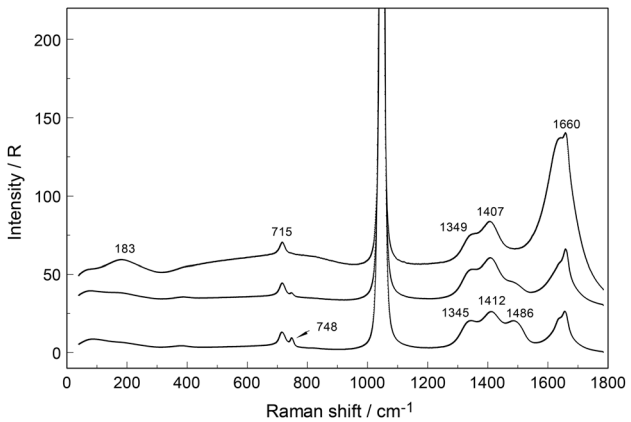

Fig. 10 Raman spectra (R-polarized) of three $Y(NO_3)_3$ solutions from bottom to top: at 2.035, 1.036 and 0.198 mol L^{-1} solute concentrations. The Raman bands in the low frequency range from 40–900 cm^{-1} at the highest and lowest solution concentration (2.035 and 0.198 mol L^{-1}) are given in greater detail in Fig. S9† (panel (A): 2.035 and (B): 0.198 mol L^{-1}). Note, that the ν_1 N–O stretching mode at ~1047 cm^{-1} is presented at its full scale in insets of Fig. S10† (panel (A): 2.035 and (B): 0.198 mol L^{-1}) for both concentrations including the bands between 1200 and 1800 cm^{-1}.

$Y(NO_3)_3$(aq) are, therefore, more complex than the ones for $NaNO_3$(aq) resulting in bands of "free" nitrate and bound nitrate. The Raman spectrum of the concentrated $Y(NO_3)_3$ solution, at 2.035 mol L^{-1}, may illustrate this (Fig. 9). The first evidence of the ligated nitrate is the split of the ν_4(e′) NO_3^- bending mode into bands at 715 cm^{-1} (fwhh = 21 cm^{-1}), at 724.5 cm^{-1} (fwhh = 18.3 cm^{-1}) and 748 cm^{-1} (fwhh = 13.5 cm^{-1}). The band at 715 cm^{-1} represents the NO_3^- bending mode of "free" NO_3^-(aq) and the bands at 724.5 cm^{-1} and 748 cm^{-1} represent the bending modes of the bound nitrate. Furthermore, a very weak and broad band at ~826 cm^{-1}, normally Raman forbidden ν_2(a″$_2$), appears in the concentrated $Y(NO_3)_3$ solution (Fig. 9). The ν_1 N–O symmetric stretching band appears broadened (fwhh = 12.2 cm^{-1}) and slightly shifted to higher wavenumbers at 1049.3 cm^{-1} compared with the N–O stretching band in dilute $NaNO_3$(aq) solutions. A moderately weak shoulder containing ~11% of the whole band contour at lower wavenumbers is also visible at 1037 cm^{-1} (fwhh = 21 cm^{-1}). The antisymmetric stretching mode, ν_3(e′) broadens and the split of the two band components mentioned earlier widens considerably. Additional isotropic band contributions of the N–O antisymmetric stretch appear at 1328 and 1470 cm^{-1} and this is shown in Fig. 9 and S10.† Finally, the Raman active overtone $2\nu_2$, which is broadened, appears at 1658 cm^{-1}. All these features appear in concentrated $Y(NO_3)_3$(aq) solutions and are clear indications that NO_3^- penetrated into the first hydration sphere of Y^{3+}. With dilution the bands of the bound nitrate disappear rapidly and are vanished in dilute solutions (Fig. 10). It is noteworthy to mention that Cabaco *et al.*[16] could not detect inner-sphere nitrato-complexes in a concentrated $Y(NO_3)_3$ at 2.89 mol L^{-1} using XRD analysis and Raman spectroscopy (no R-normalized Raman spectra have been used).

In the aqueous $Y(NO_3)_3$(aq), the weak symmetric stretching mode Y–O at 384 cm^{-1} shows a dependence on $Y(NO_3)_3$ concentration. With an increase in $Y(NO_3)_3$ concentration the band shifts to lower wavenumbers, namely from 384 cm^{-1} in dilute solutions to 379 cm^{-1} in a 2.035 mol L^{-1} solution and the band broadens as well with increasing concentration. For quantitative purposes, the broad ν_1Y–O band was fitted with two Gauss–Lorentz bands resulting in a component at 384 cm^{-1} (fwhh = 51.6 cm^{-1}) indicative of the octa-aqua yttrium^{3+} species while the second band component at 347 cm^{-1} (fwhh = 84 cm^{-1}) is due to the hydrated yttrium–nitrato complex, $[Y(OH_2)_{8-n}(NO_3)_n]^{+3-n}$. The results of the curve fit are given in Fig. 11. The ligand mode of the nitrato-complex appears as a polarized band at 223 cm^{-1}. In the concentrated solution, 45% of Y^{3+} exists in the form of a nitrato-complex. With dilution the nitrato-complex formation diminishes quickly and in the dilute solution at 0.198 mol L^{-1} only ~10% of Y^{3+} is coordinated by nitrate. Upon further dilution the nitrato-complex disappears and from extrapolations of α-values (the degree of nitrato-complex formation) as a function of solution concentration, it becomes obvious that in solutions <0.1 mol L^{-1} 99% of the Y^{3+} is fully hydrated and the nitrato-complex with only ~1% becomes insignificant. The nitrate is tentatively assumed to be monodentate, although in solid state compounds of hydrated $Y(NO_3)_3$ such as $Y(OH_2)_4(NO_3)_3{\cdot}2H_2O$ nitrate occurs in bidentate fashion.[61] It may be deduced from the work by Dobler *et al.*[62] investigating Ln(III) cations interacting with NO_3^-, that in aqueous solution with enough water to fully hydrate the trivalent cation Ln(III) (Ln = Lu^{3+}) nitrate acts as a monodentate ligand. A second shell of water molecules stabilizes the first water sphere *via* hydrogen bond formation including the nitrate. Therefore,

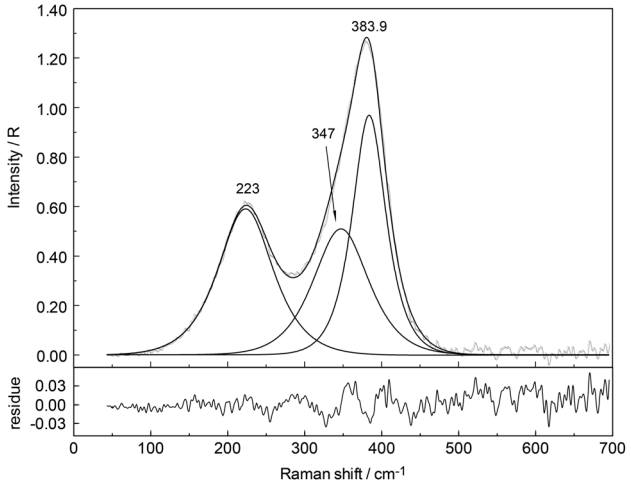

Fig. 11 Isotropic Raman spectrum (*R*-format) of 2.035 mol L^{-1} $Y(NO_3)_3$ solution in the terahertz frequency range (40–700 cm^{-1}). Given are the measured spectrum (darker line), the sum curve and the component bands of the fit at 223 cm^{-1} (fwhh = 165 cm^{-1}; A_1 = 58.02), 347 cm^{-1} (fwhh = 165 cm^{-1}; A_2 = 49.6) and 384 cm^{-1} (fwhh = 51.6 cm^{-1}; A_3 = 59.3). The index i denotes the integrated band intensities of the band intensities A_i (i = 1–3). Note the residue curve as the difference between measured curve and sum curve is given underneath.

the formation of the nitrato-complex with Y^{3+} may be expressed by eqn (8):

$$[Y(OH_2)_8]^{3+} + NO_3^- \leftrightarrow [Y(OH_2)_7ONO_2]^{2+} + H_2O. \quad (8)$$

and in a possible second step the formation of a di-nitrato complex in concentrated solutions (9):

$$[Y(OH_2)_7ONO_2]^{2+} + NO_3^- \leftrightarrow [Y(OH_2)_6(ONO_2)_2]^{+} + H_2O. \quad (9)$$

An estimate of the $\log\beta_1$ value at ~0.1 reveals the weak nature of the nitrato-complex in $Y(NO_3)_3$(aq) at 23 °C. Thermodynamic data on the weak nitrato complex formation may be found in ref. 63. Ultrasound absorption measurements were carried out on yttrium nitrate solutions applying a one-step mechanism and revealed the formation of a mono-nitrato complex.[64] The behaviour of the Y^{3+}–nitrato-complex solution is comparable to the nitrato-complex formation in $La(NO_3)_3$(aq)[26] where the complex formation is apparent albeit weak. In contrast to the weak nitrato-complex formation in aqueous $Y(NO_3)_3$, in $Al(NO_3)_3$ solutions from dilute to high concentrations, the aluminium(III) hexahydrate, $[Al(OH_2)_6]^{3+}$ exists as a stable cluster. The Raman scattering bands, especially the breathing mode at 525 cm^{-1}, indicate the existence of the hexahydrate.[58] In concentrated solutions outer-sphere ion pairs, $[Al(OH_2)_6]^{3+}\cdot NO_3^-$ are formed. However, nitrate does not penetrate the first hydration shell of Al^{3+} indicated by the unchanged Raman signature of the AlO_6 of $[Al(OH_2)_6]^{3+}$.[58]

4. Conclusions

Raman spectra of aqueous Y^{3+} perchlorate, triflate, chloride and nitrate solutions were measured over a broad concentration range (0.198 mol L^{-1}–3.252 mol L^{-1}). The terahertz frequency range has been measured as well as spectra in the O–H stretching region. The weak, polarized mode at 384 cm^{-1} (fwhh = 50 cm^{-1}) was assigned to ν_1Y–O of the YO_8 skeleton. In deuterated $Y(ClO_4)_3$ solution, a mode at 365 cm^{-1} was assigned to the breathing mode, ν_1Y–O of the $[Y(OD_2)_8]^{3+}$. Raman spectroscopic data suggest that the $[Y(OH_2)_8]^{3+}$ ion is thermodynamically stable in dilute perchlorate and triflate solutions. But inner-sphere complexes could not be detected, spectroscopically. Outer-sphere ion pairs of the type $[Y(OH_2)_8]^{3+}\cdot ClO_4^-$ and possibly inner-sphere ion pairs are formed in concentrated $Y(ClO_4)_3$(aq). DFT frequency calculations of a $[Y(OH_2)_8]^{3+}$ imbedded in a polarizable dielectric continuum gave a ν_1 Y–O equal to 372 cm^{-1} in fair agreement with the experiment. Bond distances and angles of the $[Y(OH_2)_8]^{3+}$ imbedded in a polarizable dielectric continuum were also presented. The symmetry of the octa-aqua complex is S_8 while the YO_8 skeleton has D_{4d} symmetry.

In YCl_3 solutions, Cl^- penetrates the first hydration sphere of Y^{3+}(aq) and chloro-complexes are formed. However, the chloro-complexes disappear rapidly upon dilution and at a concentration <0.2 mol L^{-1} the chloro-complexes have almost vanished. This Raman spectroscopic finding is substantiated from recent results applying neutron – and X-ray scattering as well as EXAFS.[12,16]

In concentrated $Y(NO_3)_3$ solutions, NO_3^- penetrates the first hydration sphere of Y^{3+} and a nitrato-complex was characterized; the nitrato-complex disappears fairly rapidly upon dilution and in solutions <0.1 mol L^{-1} no nitrato-complexes could be observed.

Appendix A

The binding energy for the cluster in the gas phase consisting of Y^{3+} ion with 8 water molecules in the first sphere was calculated according to eqn (10):

$$\Delta E_e = E_e[Y(OH_2)_8(g)]^{3+} - E_e[Y^{3+}(g)] - 8\cdot E_e[OH_2(g)]. \quad (10)$$

This equation corresponds to a gas-phase reaction at T = 0 K of isolated molecules with stationary nuclei, but thermochemical measurements are carried out with vibrating molecules usually at 298 K. Comparison of the theoretical with experimental data, therefore, requires correction for the translational, rotational and vibrational energy. For one mole molecules of an ideal gas, one obtains the enthalpy:

$$H(T) = E_e + E_t(T) + E_r(T) + E_v(T) + RT. \quad (11)$$

Here, E_e stands for the electronic energy, $E_t(T)$ the translational energy, $E_r(T)$ the rotational energy, and $E_v(T) = Nh\sum_i \nu_i\left(1/2 + 1/\left(e^{h\nu_i/kT} - 1\right)\right)$ is the thermal vibrational energy. The gas-phase hydration enthalpy

$\Delta H_{hyd(g)}(T)$ is then obtained with an equation similar to eqn (10). Using results of our DFT calculations and harmonic frequencies, we obtain for the cluster $[Y(OH_2)_8]^{3+}$ the standard hydration enthalpy $\Delta H_{hyd(g)}$ (298) = −2541 kJ mol^{-1} in the gas phase. The estimation of the hydration enthalpy in the liquid state, $\Delta H_{hyd(l)}$ for $[Y(OH_2)_6]^{2+}$ requires consideration of additional contributions. According to a Born-Haber cycle it follows:

$$\Delta H_{hyd(l)} \approx \Delta H_{hyd(g)} + \Delta H_{vap} + \Delta H_{solv}. \quad (12)$$

Here, ΔH_{vap} is the heat of water vaporization[65] and ΔH_{solv} means the solvation energy resulting from the transfer of the gas phase cluster to the liquid state. The solvation enthalpy of the cluster can be estimated with the Polarized Continuum Model by placing the $[Y(OH_2)_6]^{3+}$ gas phase cluster in a polarizable dielectricum and so taking implicitly into account the bulk water and comparing with the naked cluster. From the difference of the calculated enthalpies, the solvation energy ΔH_{solv} (298) results in −1762 kJ mol^{-1}. Taking into account the vaporization heat of the 8 water molecules, we obtain for the hydration enthalpy $\Delta H_{hyd(l)}$ (298) = −3951 kJ mol^{-1}.

Experimental values for the standard molar hydration enthalpy $\Delta H_{hyd(l)}$ (298) of Y^{3+} in the liquid state are: −3710 kJ mol^{-1},[37] −3599 kJ mol^{-1},[38] −3733 kJ mol^{-1},[39] −3583 kJ mol^{-1},[40] −3590 kJ mol^{-1},[41] −3620 kJ mol^{-1}.[42] The correspondence with the theoretical values is satisfactory in consideration of the simple set of basis functions that has been used.

Acknowledgements

WWR and GI wish to thank Frau B. Ostermay for her skilful technical assistance.

References

1 S. Cotton, *Lanthanide and Actinide Chemistry*, John Wiley & Sons, Chichester, West Sussex, 2006.
2 J. Emsley, *Nature's Building Blocks: An A-Z Guide to the Elements, Yttrium*, Oxford University Press, Oxford, 2011, pp. 617–620.
3 V. R. Sastri, J. R. Perumareddi, V. Ramachandra Rao, G. V. S. Rayudu and J.-C. Bünzli, *Modern Aspects of Rare Earths and their Complexes*, Elsevier, Amsterdam, 2003.
4 A. Kheyfits, *Radiol. Today*, 2010, **11**, 20.
5 N. S. MacDonald, R. E. Nusbaum, G. V. Alexander, F. Ezmirlian, P. Spain and D. E. Rounds, *J. Biol. Chem.*, 1952, **195**, 837–841.
6 C.-H. Huang and Z. Bian, *Introduction in Rare Earth Coordination Chemistry: Fundamentals and Applications*, ed. C.-H. Huang, Wiley, Singapore, 2010, pp. 1–39.
7 J. McB. Harrowfield, D. L. Kepert, J. M. Patrick and A. H. White, *Aust. J. Chem.*, 1983, **36**, 483–492.
8 R. D. Rogers and L. K. Kurihara, *Inorg. Chim. Acta*, 1986, **116**, 171–177.
9 R. W. Broach, J. M. Williams, G. P. Felcher and D. G. Hinks, *Acta Crystallogr., Sect. B: Struct. Crystallogr. Cryst. Chem.*, 1979, **35**, 2317–2321.
10 F. A. Cotton, A. Davison, V. W. Day, M. F. Fredrich, C. Orvig and R. Swanson, *Inorg. Chem.*, 1982, **21**, 1211–1214.
11 Y. Ohki, Y. Suzuki, T. Takeuchi and A. Ouchi, *Bull. Chem. Soc. Jpn.*, 1988, **61**, 393–405.
12 G. Johansson and H. Wakita, *Inorg. Chem.*, 1985, **24**, 3047–3052.
13 E. Matsubara, K. Okuda and Y. Waseda, *J. Phys.: Condens. Matter*, 1990, **2**, 9133–9143.
14 M. I. Cabaco, M. A. Marques, M. I. de Barros Marques, G. Bushell-Wye, M. M. Costa, M. J. de Almeida and L. C. Andrade, *J. Phys.: Condens. Matter*, 1995, **7**, 7409–7418.
15 S. Ramos, G. W. Neilson, A. C. Barnes and A. Mazuelas, *J. Phys. Chem. B*, 2001, **105**, 2694–2698.
16 M. I. Cabaco, M. I. de Barros Marques, M. A. Marques, A. M. Gaspar and M. L. de Almeida, *J. Mol. Liq.*, 2005, **117**, 69–76.
17 M. I. de Barros Marques, M. A. Marques and J. R. Rodrigues, *J. Phys.: Condens. Matter*, 1992, **4**, 7679–7690.
18 K. V. Ragnarsdottir, E. H. Oelkers, D. M. Sherman and C. R. Collins, *Chem. Geol.*, 1998, **151**, 29–39.
19 P. Lindqvist-Reis, K. Lamble, S. Pattanaik, I. Persson and M. Sandström, *J. Phys. Chem. B*, 2000, **104**, 402–408.
20 S. Diaz-Moreno, A. Munoz-Paez and J. Chaboy, *J. Phys. Chem. A*, 2000, **104**, 1278–1286.
21 D. T. Bowron and S. Diaz-Moreno, *J. Phys. Chem. B*, 2007, **111**, 11393–11399.
22 T. Ikeda, M. Hirata and T. Kimura, *J. Chem. Phys.*, 2005, **122**, 024510–024515.
23 W. W. Rudolph, M. H. Brooker and C. C. Pye, *J. Phys. Chem.*, 1995, **99**, 3793–3797.
24 W. W. Rudolph and G. Irmer, *Dalton Trans.*, 2013, 3919–3935.
25 W. W. Rudolph and G. Irmer, *Dalton Trans.*, 2013, 14460–14472.
26 W. W. Rudolph and G. Irmer, *Dalton Trans.*, 2015, **44**, 295–305.
27 W. W. Rudolph and C. C. Pye, *Phys. Chem. Chem. Phys.*, 2002, **4**, 4319–4327.
28 W. W. Rudolph, D. Fischer, M. R. Tomney and C. C. Pye, *Phys. Chem. Chem. Phys.*, 2004, **6**, 5145–5155.
29 V. A. Sipachev and A. I. Grigor'ev, *Zh. Strukt. Khim.*, 1969, **10**, 710–714.
30 W. W. Rudolph and G. Irmer, *Appl. Spectrosc.*, 2007, **61**, 1312–1327.
31 A. I. Vogel, *A Text-Book of Quantitative Inorganic Analysis*, Longman, London, 3rd edn, 1961.
32 F. H. Spedding, M. J. Pikal and B. O. Ayers, *J. Phys. Chem.*, 1966, **70**, 2440–2449; see p. 2441.
33 W. W. Rudolph, D. Fischer and G. Irmer, *Appl. Spectrosc.*, 2006, **60**, 130–144.

34 M. J. Frisch, G. W. Trucks, H. B. Schlegel, G. E. Scuseria, M. A. Robb, J. R. Cheeseman, J. A. Montgomery, Jr., T. Vreven, K. N. Kudin, J. C. Burant, J. M. Millam, S. S. Iyengar, J. Tomasi, V. Barone, B. Mennucci, M. Cossi, G. Scalmani, N. Rega, G. A. Petersson, H. Nakatsuji, M. Hada, M. Ehara, K. Toyota, R. Fukuda, J. Hasegawa, M. Ishida, T. Nakajima, Y. Honda, O. Kitao, H. Nakai, M. Klene, X. Li, J. E. Knox, H. P. Hratchian, J. B. Cross, V. Bakken, C. Adamo, J. Jaramillo, R. Gomperts, R. E. Stratmann, O. Yazyev, A. J. Austin, R. Cammi, C. Pomelli, J. W. Ochterski, P. Y. Ayala, K. Morokuma, G. A. Voth, P. Salvador, J. J. Dannenberg, V. G. Zakrzewski, S. Dapprich, A. D. Daniels, M. C. Strain, O. Farkas, D. K. Malick, A. D. Rabuck, K. Raghavachari, J. B. Foresman, J. V. Ortiz, Q. Cui, A. G. Baboul, S. Clifford, J. Cioslowski, B. B. Stefanov, G. Liu, A. Liashenko, P. Piskorz, I. Komaromi, R. L. Martin, D. J. Fox, T. Keith, M. A. Al-Laham, C. Y. Peng, A. Nanayakkara, M. Challacombe, P. M. W. Gill, B. Johnson, W. Chen, M. W. Wong, C. Gonzalez and J. A. Pople, *Gaussian 03, Revision C.02*, Gaussian, Inc., Wallingford CT, 2004.
35 C. Lee, W. Yang and R. C. Parr, *Phys. Rev. B: Condens. Matter*, 1988, **37**, 785–789.
36 M. Cossi, G. Scalmani, N. Rega and V. Barone, *J. Chem. Phys.*, 2002, **117**, 43–54.
37 R. Noyes, *J. Am.. Chem. Soc.*, 1962, **84**, 513–522.
38 D. R. Rosseinsky, *Chem. Rev.*, 1965, **65**, 467–490.
39 J. E. Desnoyers and C. Jolicoeur, in *Modern Aspects of Electrochemistry*, ed. J. O'M. Bockris and B. E. Conway, Plenum Press, New York, N. Y., 1969, ch. 1, vol. 5.
40 D. W. Smith, *J. Chem. Educ.*, 1977, **54**, 540–542; D. W. Smith, *J. Chem. Educ.*, 1977, **54**, 540–542.
41 Y. Marcus, *Biophys. Chem.*, 1994, **51**, 111–127.
42 J. Burgess *Ions in Solution: Basic Principles of Chemical Interactions*, Ellis Horwood, Chichester/Halsted Press, New York, 1988.
43 W. Rudolph and S. Schönherr, *Z. Phys. Chem.*, 1989, **270**, 1121–1134.
44 B. Auer, R. Kumar, J. R. Schmidt and J. L. Skinner, *Proc. Natl. Acad. Sci. U. S. A.*, 2007, **104**, 14215–14220.
45 B. M. Auer and J. L. Skinner, *J. Chem. Phys.*, 2008, **128**, 224511.
46 M. H. Brooker, G. Hancock, B. C. Rice and J. Shapter, *J. Raman Spectrosc.*, 1989, **20**, 683–694.
47 N. Purdie and C. A. Vincent, *Trans. Faraday Soc.*, 1967, **63**, 2745–2757.
48 D. P. Fay, D. Litchinsky and N. Purdie, *J. Phys. Chem.*, 1969, **73**, 544–552.
49 G. E. Walrafen, *J. Chem. Phys.*, 1962, **36**, 1035–1042.
50 I. A. Heisler, K. Mazur and S. R. Meech, *J. Phys. Chem. B*, 2011, **115**, 1863–1873.
51 C. Cossy, L. Helm and A. E. Merbach, *Inorg. Chem.*, 1989, **28**, 2699–2703.
52 L. Helm and A. E. Merbach, *Chem. Rev.*, 2005, **105**, 1923–1959.
53 J. Zhang, N. Heinz and M. Dolg, *Inorg. Chem.*, 2014, **53**, 7700–7708.
54 R. D. Shannon, *Acta Crystallogr., Sect. A: Cryst. Phys., Diffr., Theor. Gen. Cryst.*, 1976, **32**, 751–767.
55 G. D. Klungness and R. H. Byrne, *Polyhedron*, 2000, **19**, 99–107.
56 X. Liu, X. Lu, R. Wang and H. Zhou, *Chem. Geol.*, 2012, **334**, 37–43.
57 R. G. Pearson, *J. Am. Chem. Soc.*, 1963, **85**, 3533–3539.
58 W. W. Rudolph, R. Mason and C. C. Pye, *Phys. Chem. Chem. Phys.*, 2000, **2**, 5030–5040.
59 K. A. Kraus, F. Nelson and G. W. Smith, *J. Phys. Chem.*, 1954, **58**, 11–17.
60 J. Thøgersen, J. Réhault, M. Odelius, T. Ogden, N. K. Jena, S. J. Jensen, S. R. Keiding and J. Helbing, *J. Phys. Chem. B*, 2013, **117**, 3376–3388.
61 B. Ribar, N. Milinski and Z. Budovalcev, *Cryst. Struct. Commun.*, 1980, **9**, 203–206.
62 M. Dobler, P. Guilbaud, A. Dedieu and G. Wipff, *New J. Chem.*, 2001, **25**, 1458–1465.
63 J. Schijf and R. H. Byrne, *Geochim. Cosmochim. Acta*, 2004, **68**, 2825–2837.
64 H. Wang and P. Hemmes, *J. Phys. Chem.*, 1974, **78**, 261–265.
65 J. D. Cox, D. D. Wagman and V. A. Medvedev, *CODATA Key Values for Thermodynamics*, Hemisphere Publishing Corp., New York, 1989.